doi:10.26443/seismica.v2i2.1030

Optimal Network Design for Microseismic Monitoring in Urban Areas - A Case Study in Munich, Germany

Sabrina Keil * [1], **Joachim Wassermann** [1], **Tobias Megies** [1], **Toni Kraft** [2]

[1]Ludwig-Maximilians-Universität München, Germany, [2]Swiss Seismological Service, ETH-Zurich, Switzerland

Author contributions: *Software*: T. Megies, T. Kraft. *Formal Analysis*: S. Keil. *Writing - original draft*: S. Keil. *Writing - Review & Editing*: J. Wassermann, T. Megies, T. Kraft. *Visualization*: S. Keil. *Supervision*: J. Wassermann.

Abstract Well-designed monitoring networks are crucial for obtaining precise locations, magnitudes and source parameters, both for natural and induced microearthquakes. The performance of a seismic network depends on many factors, including network geometry, signal-to-noise ratio (SNR) at the seismic station, instrumentation and sampling rate. Therefore, designing a high-quality monitoring network in an urban environment is challenging due to the high level of anthropogenic noise and dense building infrastructure, which can impose geometrical limitations and elevated construction costs for sensor siting. To address these challenges, we apply a numerical optimization approach to design a microseismic surveillance network for induced earthquakes in the metropolitan area of Munich (Germany), where several geothermal plants exploit a deep hydrothermal reservoir. First of all, we develop a detailed noise model for the city of Munich, to capture the heterogeneous noise conditions. Then, we calculate the expected location precision for a randomly chosen network geometry from the body-wave amplitudes and travel times of a synthetic earthquake catalog considering the modeled local noise level at each network station. In the next step, to find the optimum network configuration, we use a simulated annealing approach in order to minimize the error ellipsoid volume of the linearized earthquake location problem. The results indicate that a surface station network cannot reach the required location precision (0.5 km in epicentre and 2 km in source depth) and detection capability (magnitude of completeness M_c = 1.0) due to the city's high seismic noise level. In order to reach this goal, borehole stations need to be added to increase the SNR of the microearthquake recordings, the accuracy of their body-wave arrival times and source parameters. The findings help to better quantify the seismic monitoring requirements for a safe operation of deep geothermal projects in urban areas.

Production Editor: Gareth Funning
Handling Editor: Yen Joe Tan
Copy & Layout Editor: Théa Ragon

Signed reviewer(s): Anthony Lomax

Received: June 5, 2023
Accepted: October 5, 2023
Published: October 18, 2023

1 Introduction

The main purpose of seismic networks is to determine earthquake locations and magnitudes, which is important for earthquake characterization, hazard assessment and emergency response both for natural and induced seismicity (e.g., Havskov et al., 2012; Lomax et al., 2009). Specifically, induced seismicity caused by geothermal energy production is a growing concern, since the number of geothermal projects is raising in search of carbon-free heat and electricity generation (Hirschberg et al., 2014; Lund and Toth, 2021). In most cases the induced events have small magnitudes ($M_L < 2$) and are not felt by the local population (Evans et al., 2012). However, examples like the Deep Heat Mining Project in Basel, Switzerland (Häring et al., 2008), and geothermal projects near Strasbourg, France (Schmittbuhl et al., 2021), where induced events with magnitudes $M_L > 3$ were recorded, highlight the importance of managing the induced seismicity risk. Consequently, a good monitoring network is a necessary component of the risk governance strategy to detect and locate small magnitude earthquakes, which enable the functioning of magnitude-based traffic light systems (Kraft et al., 2020). The precision of earthquake location depends on several factors, such as the distribution of seismic stations, detection of seismic waves and the accuracy of their observed and calculated arrival times (e.g., Bondár et al., 2004; Havskov et al., 2012). However, low-SNR recordings hamper the detection of small magnitude events and lead to high location uncertainties, which result in a poor performance of the monitoring network (e.g., Bormann and Wielandt, 2013). This is especially an issue in urban areas where often high seismic noise levels are encountered. Even though, well-designed monitoring networks are fundamental to allow the detection of weak seismic signals, seismic network planning is still mainly performed as a manual task based on simple design rules, which may fail in complex settings. Several different approaches have been proposed for the improvement of seismic networks including 1) the computation of the expected location errors and lowest detectable magnitude (Stabile et al., 2013; De Landro et al., 2020), 2) seismic network evaluation through simulation (e.g., D'Alessandro et al., 2011; Mahani et al., 2016), 3) correction of teleseismic travel times (e.g., Myers and Schultz, 2000), and 4) implementation of the D-criterion to identify an optimal seismic network configuration to decrease the location error (e.g., Steinberg

*Corresponding author: skeil@geophysik.uni-muenchen.de

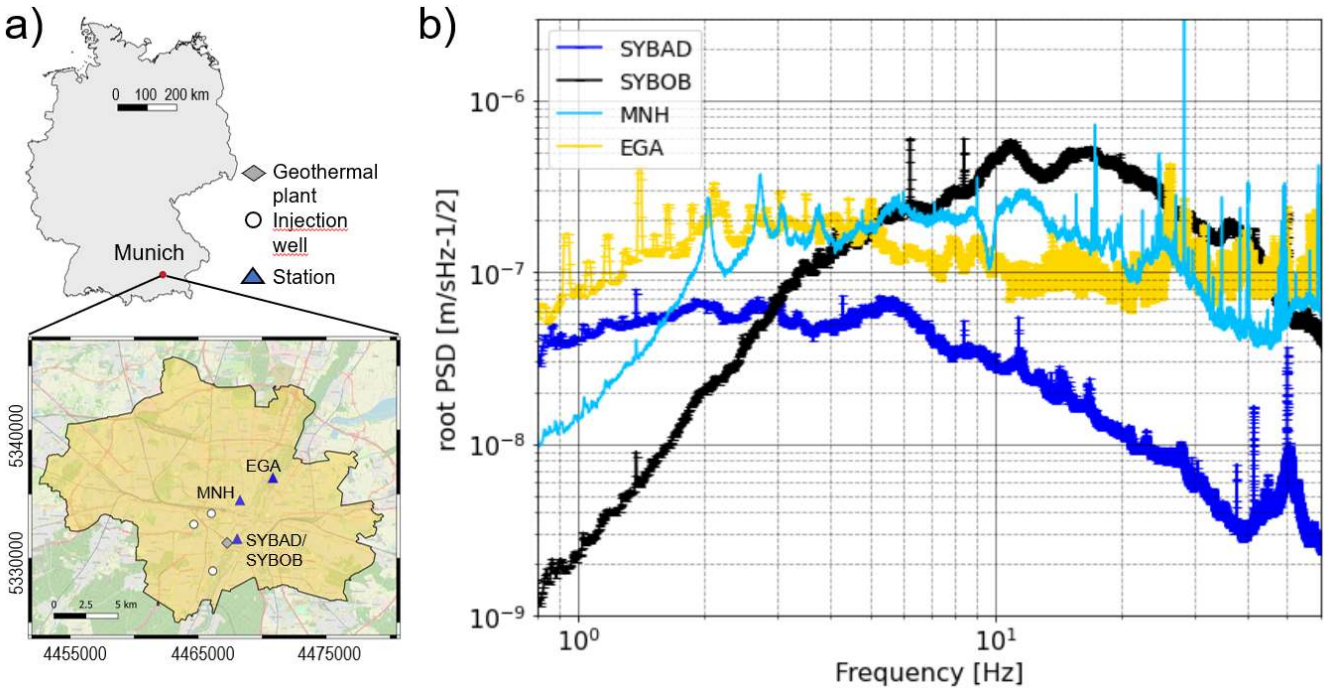

Figure 1 a) The upper map shows an overview of Germany with the location of Munich marked. The lower map shows an overview of the Munich city with the geothermal power plant at Schäftlarnstraße and its three injection wells. The locations of several seismic stations in Munich are marked. SYBAD corresponds to a 180m-deep borehole station and SYBOB is its overlying surface station. MNH is a permanent surface station and EGA was temporarily installed within a park area. At SYBOB a 4.5 Hz geophone is installed, at MNH a Mark L4-3D 1 Hz seismometer, at EGA a Trillium Compact 120s seismometer, and at SYBAD a Trillium Compact PH 20s seismometer. The coordinate system is Gauss-Krüger (GK4). b) Root Power spectral density (PSD) plots of data recorded at the seismic stations marked in a). The PSDs were computed from the vertical component for one day of data.

and Rabinowitz, 2003; Kijko, 1977). In the last case, the optimization problem can be solved using genetic algorithm techniques (e.g., Bartal et al., 2000), simulated annealing (e.g., Hardt and Scherbaum, 1994; Kraft et al., 2013), or Bayesian techniques (e.g., Coles and Curtis, 2011).

In this study we are applying the method of Kraft et al. (2013), which builds on the simulated annealing approach proposed by Hardt and Scherbaum (1994). This approach allows the optimization of seismic networks in complex settings, taking into account user-specified velocity models and heterogeneous noise conditions, as well as already existing monitoring stations. The program returns expected location uncertainties and detection thresholds of the resulting network.

We apply this method to the metropolitan area of Munich (Fig. 1 a), where currently 17 deep geothermal power plants operate (Agemar et al., 2014). This includes the geothermal project in Schäftlarnstraße (SLS), which is located in Munich's inner-city with a total of six deep wells (3 production, 3 re-injection) and a footprint of several square kilometers (Lentsch and Schweingruber, 2022). Since induced earthquakes were observed at surrounding geothermal power plants with magnitudes up to 2.4 (Megies and Wassermann, 2014; Seithel et al., 2019), the induced seismicity risk needs to be considered also at this recently realized project, which rises the requirement for a high quality monitoring network. The monitoring network for the geothermal power plants south of Munich was already optimized during the MAGS2 project (Megies and Wassermann, 2017), however, the inner-city project SLS had not been constructed at that time.

Since the number of geothermal projects in Germany is growing and consequently the risk of induced seismicity increases, Baisch et al. (2012) proposed a number of seismic monitoring recommendations for induced seismicity for the German Research College Physics of the Earth (FKPE). They recommend a monitoring network that is able to reliably detect and locate all earthquakes with magnitudes $M_L \geq 1$ with epicentral uncertainties of less than 500 m and vertical uncertainties of less than 2 km. These thresholds should be reached in an area of 5 km surrounding the target areas of the geothermal project. For the following quality assessment of the monitoring network in the Munich area, we are taking these recommendations into account.

First of all, we construct a detailed model of anthropogenic noise in the metropolitan region of Munich to capture its heterogeneous noise conditions. In the next step the quality of the existing monitoring network is evaluated according to the FKPE recommendations. Afterwards, a number of numerical network optimization runs are performed that test how the FKPE recommendations can be met by adding new surface and boreholes stations to the existing network.

2 Methodology

For the network optimization, we use a simulated annealing code initially developed by Hardt and Scherbaum (1994) that was substantially extended by Kraft et al. (2013) (hereafter referred to as NetOpt3D). Due to license issues, NetOpt3D was recently rewritten by Antuens et al. (2023) using open software libraries. For the current analysis, the python wrapper pyNetOpt3D (Megies et al., 2023) was built around the binaries of Antuens et al. (2023) to handle the input and output of the optimization code more easily. In the following, we briefly describe the concept of NetOpt3D and pyNetOpt3D.

NetOpt3D finds the D-optimal design by minimizing the volume of the error ellipsoid of the linearized earthquake location problem (D-criterion, e.g., Kijko, 1977) using a simulated annealing approach (Kirkpatrick et al., 1983). The simulated annealing parameters (e.g. starting temperature, minimum temperature, cooling schedule, maximum number of temperature steps, temperature reduction by step, and trials per step) were fine-tuned by trial and error in order to achieve a slow and smooth convergence of the solution to the global minimum. In order to solve the optimization problem the program computes traveltimes of seismic body waves using the finite difference ray tracer of Podvin and Lecomte (1991) and a user-defined velocity model. Furthermore, to evaluate the detectability of an event at the seismic stations body wave amplitudes are calculated based on earthquake source processes and wave propagation effects. Path effects are only treated in an approximate way by geometrical spreading, constant attenuation and free-surface amplification. The Brune model (Brune, 1970) is implemented as seismic source. The SNR is defined as the ratio of the synthetic body wave amplitude and the observed or estimated long-term root-mean-squared ground velocity at the station. We choose a SNR of 5 as the threshold for an earthquake to be observed at a certain station. In general a SNR ≥ 3 is considered being sufficient to reliably detect a seismic phase onset in a seismogram (e.g., Hardt and Scherbaum, 1994; Baisch et al., 2012). However, we chose a more conservative threshold as the estimated signal amplitude in our optimization approach corresponds to the maximum expected amplitude of the considered body wave at the recording station, which may be significantly larger than the amplitude of the phase onset (Kraft et al., 2013). We utilize the estimated SNR of a seismic phase at a station to calculate the expected uncertainty of the phase's onset time following the approach of Aki (1976) based on information theory (Shannon, 1948). According to Shannon (1948) a simple relation for the estimation of the information content of a signal exists:

$$WTlog_2\frac{S^2+N^2}{N^2} \quad (1)$$

where S^2 and N^2 represents the power of signal and noise, respectively, and T is the duration of the time series. The signal bandwidth W is approximated by max(fc, fmax). Here fc represents the Brune corner frequency of the event, and fmax corresponds to the high-frequency band limitation of the radiated field, as estimated from the attenuation model of Edwards et al. (2011) for Switzerland. More details about the NetOpt3D program, including the annealing schedule and the calculation of body wave traveltimes and amplitudes are given in Kraft et al. (2013).

In its current form, NetOpt3D is lacking usability and it is time consuming to set up new optimization problems. Input files (e.g. velocity models, synthetic earthquake catalogs) have to be set up manually in fixed legacy ASCII formats defined by the underlying C codes and a large number of helper programs (e.g. Linux shell scripts) are used for preparational steps and for analysis and visualization of results. Therefore, the consistent and easy-to-use Python Application Programming Interface (API) pyNetOpt3D was developed that internally uses NetOpt3D C codes but hides all unwieldy steps from the user. It enables the start of a complete optimization run with a single, short Python script using the newly developed API. All coordinate conversions from global geographic coordinates (WGS84) to local geodetic coordinates (e.g. UTM, Gauß-Krüger, Swiss Grid, ...) and vice versa are handled automatically. Functionalities to calculate convex hulls, buffers and equistant station grids are included. It also enhances reproducibility by providing (de)serialization of a full optimization run including all input data and results into a single file. Furthermore, pyNetOpt3D provides command line tools to quickly plot optimization results from a serialized file on disk.

In order for the NetOpt3D program to perform the optimization, a number of user-specified input data is required, which will be discussed in detail in the next sections.

3 Ambient Noise Analysis

The detectability of an event at a specific station depends on the amplitude of the earthquake signal and the noise level at the site. Therefore, an estimate of the background noise at the existing stations and the potential new network sites is required. First of all, we investigate the frequency content of the seismic noise by computing power spectral densities (PSD) at several stations located in the Munich city (Fig. 1). The surface station SYBOB[1] clearly shows higher PSD values for frequencies above 3 Hz compared to the underlying 180m-deep borehole station SYBAD. The highest power at SYBOB is observed between 10-20 Hz, while the PSD values at SYBAD decrease for frequencies above 6 Hz. The PSD values of the surface station MNH are high for frequencies larger than 2 Hz. Above 5 Hz the temporary installed station EGA displays PSD values lower than SYBOB and MNH, which can be explained by the installation within a park area. From these observations it can be inferred that the anthropogenic noise sources (e.g. trains, vehicles, construction work, industrial operation) influence the noise amplitudes at high frequencies (>1 Hz), which is consistent with findings of other

[1]Note that at SYBOB a 4.5 Hz geophone is installed, therefore the data should not be interpreted for frequencies much lower than 4.5 Hz.

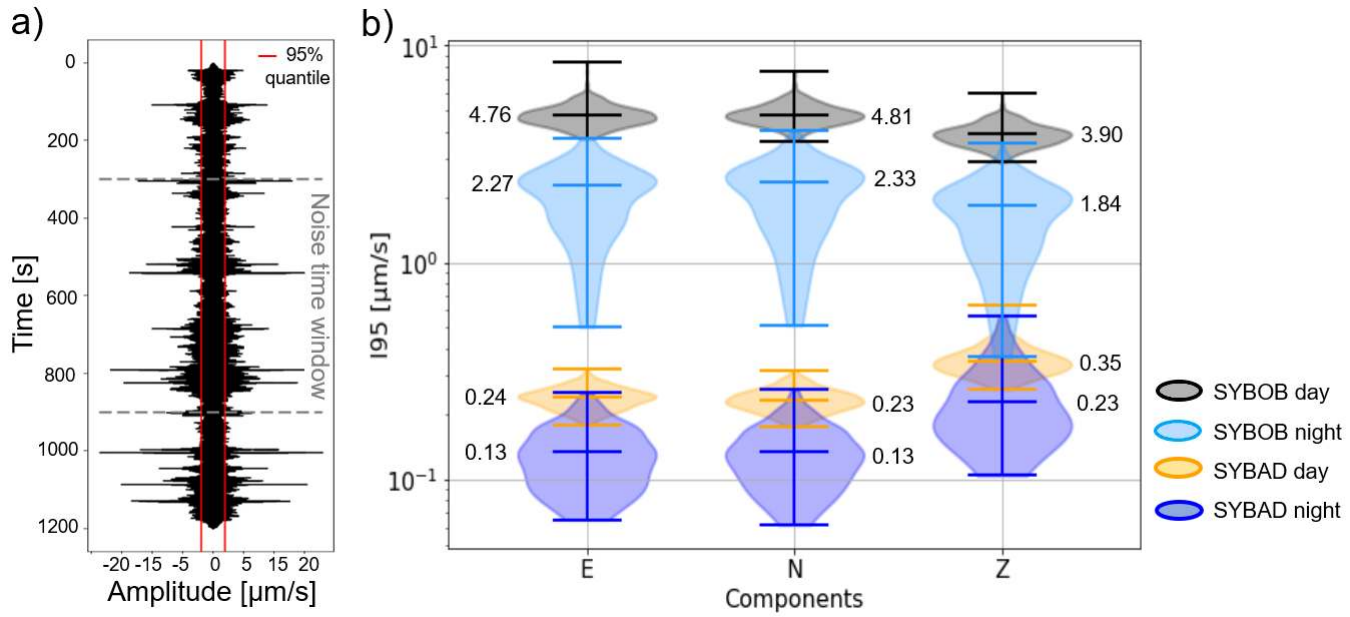

Figure 2 a) Seismic noise recorded at the surface station SYBOB in Munich in a frequency range of 1 - 20Hz. The 95% quantile of the data is shown by the red lines. The I95 value is computed from the 95% quantiles for 10 minute time windows. b) Violin plots of I95 values calculated at the surface station SYBOB and the underlying 180m-deep borehole station SYBAD for the east (E), north (N) and vertical (Z) component. The I95 values were calculated over 5 working days (Monday - Friday) in 10 minute time windows and were separated into daytime (6am - 10pm) and nighttime (10pm - 6am). The median values are marked in the plot.

authors (e.g., Asten and Henstridge, 1984; Groos and Ritter, 2009). In addition, the noise amplitudes at the seismic station can be reduced through installation in boreholes and more isolated areas, like parks and green spaces.

Another measure to evaluate the noise level at a site is the I95 value, which represent the 95^{th} percentiles of the ground velocity amplitude recordings (Fig. 2 a). We calculate the I95 values in a frequency range of 1-20 Hz, which contains the dominant amplitudes of the cultural noise and corresponds to the main frequency range of the induced events observed in the Munich area (Megies and Wassermann, 2017). To investigate the variation of anthropogenic noise, the I95 values are computed at the surface station SYBOB and the borehole station SYBAD for 10-minute time windows during the daytime and nighttime, respectively. The computed I95 values are summed in violin plots and the median is taken as a representative value for the noise amplitude at the site (Fig. 2 b). A clear variation between daytime and nighttime is visible. For the surface station SYBOB the median noise amplitudes are reduced by a factor of 2 during the night. In addition, the noise amplitudes at the surface station SYBOB are by a factor of 10 larger for the vertical component compared to the borehole station SYBAD. This value is close to a factor of 13 that is estimated using the simple assumption that the noise level in the borehole decreases by a factor of $\sqrt{depth[m]}$. Assuming the most inconvenient noise conditions for the detection of microseismic events, we take the median I95 value during the day as a measure for the noise amplitudes at the site. In order to implement the calculated noise values into the pyNetOpt3D program the I95 values have to be converted to root-mean-square (RMS) ground velocity values. Assuming that the noise distribution is Gaussian, the I95 values can be converted by $RMS = I95/2$ (Neuffer and Kremers, 2017).

To estimate the background noise at the potential new network sites, a noise map for the Munich area has to be developed. Kraft (2014, 2016) developed an ambient seismic noise model for Europe based on land-use data derived from satellite imagery by the European Commission project CORINE (Büttner et al., 2004) and open GIS data on infrastructure from the OpenStreetMap project. The model is available for Europe in a $250m \times 250m$ resolution and divides the surface into three classes that represent good, intermediate and bad ambient noise conditions. Kraft (2014, 2016) defined following RMS bounds for each noise class: Low: $RMS \leq 30nm/s$, Middle: $30nm/s < RMS \leq 120nm/s$, High: $RMS > 120nm/s$. Almost the entire Munich city is characterized by high ambient noise values (Fig. 3). By comparing the measured noise values at the stations with the values assigned in the noise map, we see that they are mainly underestimated in the model. Therefore, for optimizing the seismic monitoring network in the urban area of Munich a more detailed noise model is required in order to capture the small-scale heterogeneous noise conditions.

We develop such a noise model for the Munich city extending the approach of Kraft (2014, 2016). First of all, land-use data from the Bavarian surveying administration (see data availability) is used to categorize the area into different classes including industrial buildings, residential buildings, sports and recreation areas, vegetation or water bodies and based on that assign a minimum noise level (Table 1). In the second step, different types of roads are identified as noise sources and sub-

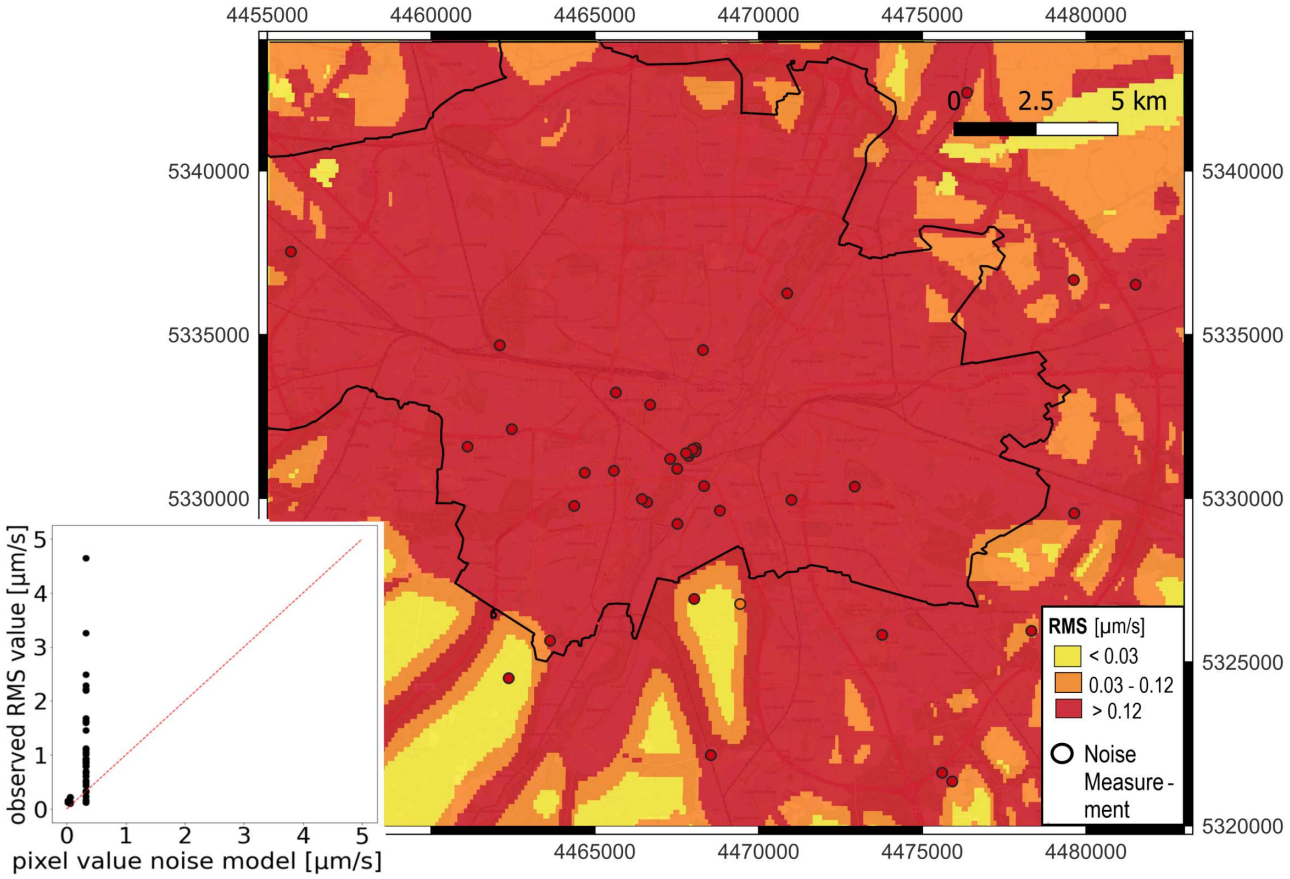

Figure 3 Noise map of Munich after Kraft (2014, 2016). The city boundary is outlined by the black line. The area is divided into three noise classes with low, intermediate and high noise values. The yellow areas are assigned a value of 0.015 µm/s, the orange areas 0.06 µm/s and the red areas a value of 0.325 µm/s. The small circles show noise measurements at permanent and temporary installed seismic stations. The coordinate system is Gauss-Krüger (GK4). In the lower left corner the observed RMS value at the seismic stations are plotted against the calculated pixel value in the noise model.

divided into different classes based on OpenStreetMap data (see data availability). Highways are assumed to have a higher noise contribution, compared to intercity roads, railways or residential streets. In order to account for noise propagation away from these sources, we implement noise-distance relations, that were derived from seismic measurements at distinct noise features (Riedl, 2017). Hereby, several seismometers were installed with increasing distance from the source to map the decreasing amplitude of the ambient vibrations. As last input traffic volume data from the city of Munich (see data availability) are implemented to adjust the noise level for busy roads. The overall noise value at one point is then calculated by adding the minimum noise level assigned from the land-use data and the noise contribution of the main sources scaled by the noise-distance relation. The resulting noise model of Munich's inner-city (Fig. 4) has a resolution of 5×5 m. To verify the calculated noise levels we compare them to the measured noise values at permanent and temporary installed stations. For sites with low noise level the calculated values are mostly close to the measured values. For sites with high noise level our model underestimates the RMS value, which is most likely due to noise sources and site effects that are not mapped into our model. As can be seen in Fig. 4, our noise model for

Table 1 Land use classes with assigned minimum I95 noise level after Riedl (2017).

Land use class	Noise value [μm/s]
Industrial usage	1.2
Housing	0.6
Sports/recreation	0.3
Vegetation, water	0.15

Munich is dominated by street traffic noise. In addition, the overall noise level in the city center is higher compared to the surroundings. Nevertheless, even within the city low noise areas are identified, which might be suitable for the installation of monitoring stations. We implement the high-resolution noise map of the Munich city into the larger-scale background noise map of Kraft (2014, 2016) for the surrounding areas.

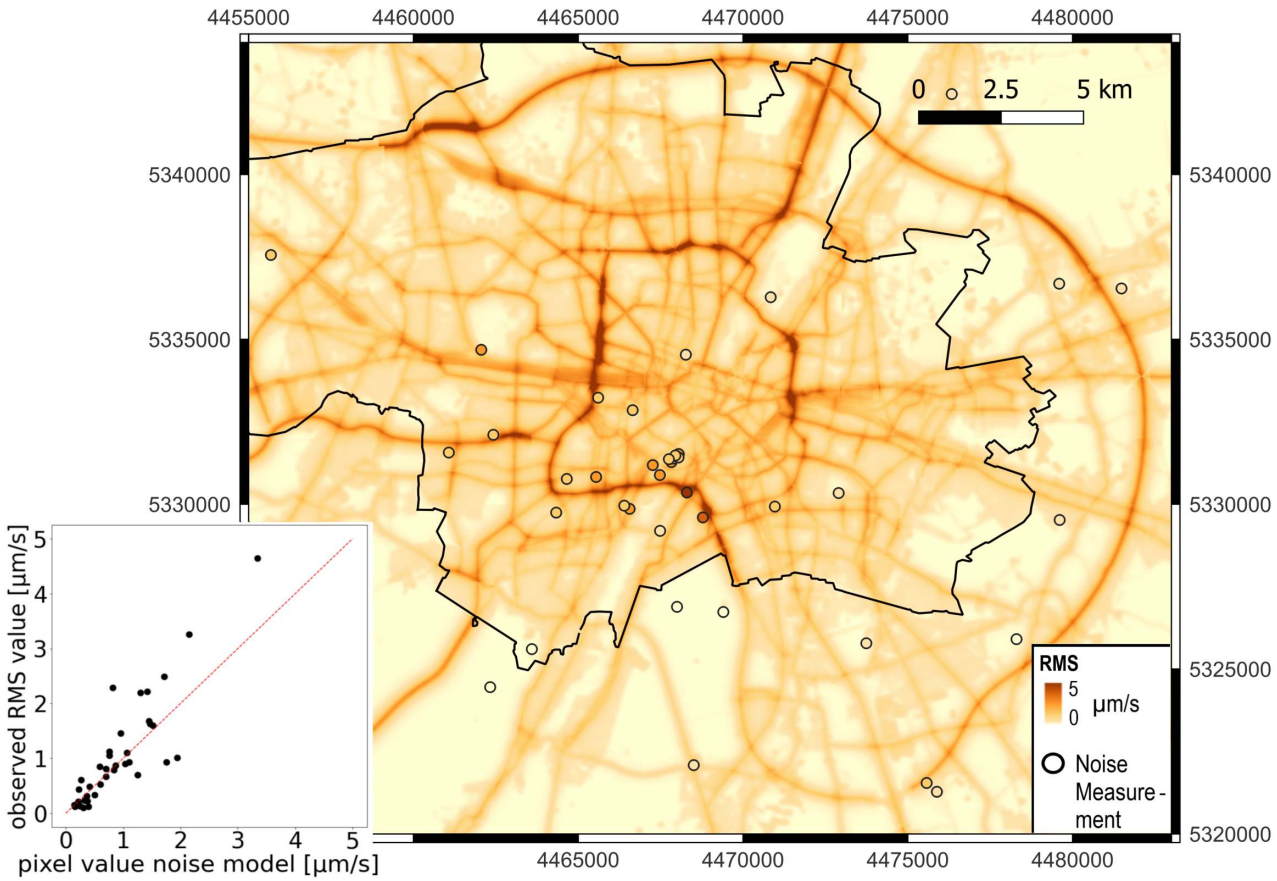

Figure 4 High-resolution noise map of Munich's inner-city. The city boundary is outlined by the black line. Colors represent the noise level, which is calculated as I95 values in a frequency range of 1-20 Hz and converted to RMS. Circles show locations of noise measurements from permanent and temporary installed seismic stations. The coordinate system is Gauss-Krüger (GK4). In the lower left corner the observed RMS value at the seismic stations are plotted against the calculated pixel value in the noise model.

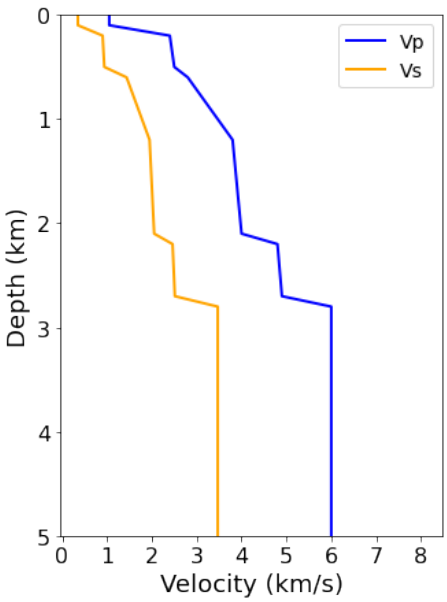

Figure 5 1D P- and S-wave velocity profiles (Vp, Vs) implemented into pyNetOpt3D for the calculation of body wave amplitudes and traveltimes.

4 Model Set-up

To calculate the signal-to-noise ratio at the potential station, we implement the high resolution noise model developed in section 3. As next step, in order to calculate body wave traveltimes, a velocity model has to be implemented. In the Munich area, information on the boundaries of the main geological units are available from a structural model developed by the Bavarian State Office for Environment (Bayerisches Landesamt für Umwelt, 2012). The P-wave velocities within the layers are based on a 3D seismic survey conducted in 2015/16 as part of the GRAME project (Hecht and Pletl, 2015), which covered 170 km^2 in the southern and western parts of Munich. The S-wave velocities are calculated from Vp/Vs ratios found by Wawerzinek et al. (2021) for the Munich area. The NetOpt3D program is able to implement 3D velocity models, however, in this study we only consider a 1D velocity profile (Fig. 5) since we assume that 3D effects only have a minor influence on the results.

Seismic waves attenuate while propagating and their amplitudes usually decrease with propagation distance. To account for seismic attenuation, we implement the attenuation model of Eulenfeld and Wegler (2016) for the geothermal project in Unterhaching south of Munich, since the ray geometry and geologic setting at this

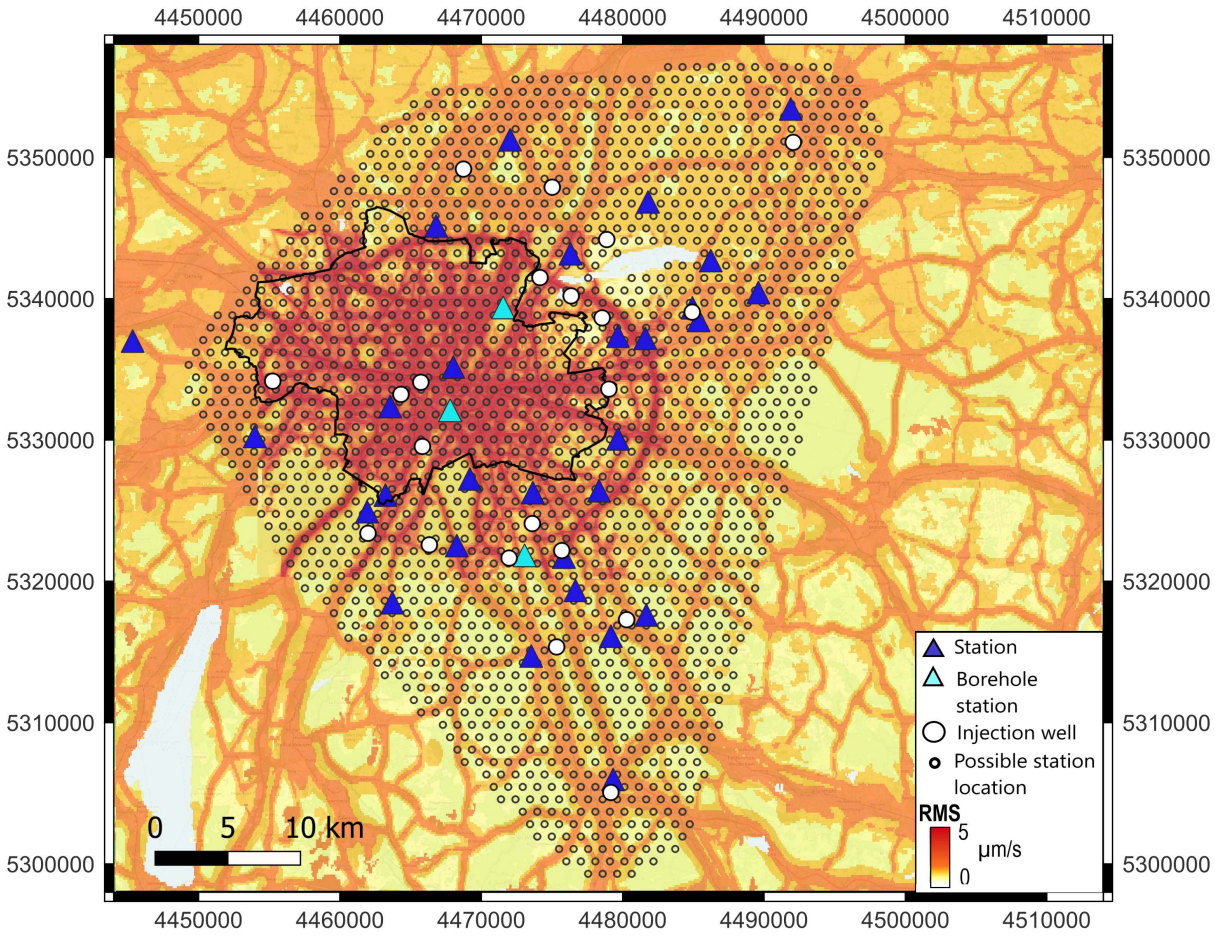

Figure 6 Set-up of the input data for the network optimization program. The Munich city boundary is outlined by the black line. Existing surface and borehole stations, as well as location of injection wells are plotted. The event locations are placed at the injection wells. The colors show the computed background noise level as RMS ground velocity. Small circles represent schematically the grid of possible station locations that can be selected during the optimization process. The coordinate system is Gauss-Krüger (GK4).

site is very similar to the one expected for other locations in the study area. They estimated a mean S-wave quality factor (Qs) of 100 averaged over the whole ray path, which is constant for frequencies lower than 8 Hz. Due to the lack of further information on the attenuation of P-waves, we set the P-wave quality factor (Qp) to 200, as literature suggests that Qp is approximately two times higher than Qs (e.g., Fowler, 1990).

For the network optimization a synthetic earthquake catalogue has to be generated. We place the events in the crystalline basement at 3 - 4 km depth underneath the re-injection wells of the geothermal power plants, as most of the recorded induced seismicity occurred close to these locations (Megies and Wassermann, 2014; Seithel et al., 2019). The focal mechanisms for the events were chosen to resemble those of the known induced earthquakes and the fault geometry in the study area, which generally corresponds to left-lateral strike-slip mechanisms with normal faulting component. We implement the events with M_W 1.3, which was converted from M_L 1.0 according to the relation found by Grünthal and Wahlström (2003) for earthquakes in central Europe.

As the optimization algorithm is able to take already existing stations into account, we implement the existing surface and borehole stations in the area with their observed noise levels.

As a last step, we have to define the geographical region for possible new station locations. We set the station perimeter with a maximum distance of 8 km to the earthquake epicenters, which corresponds to approximately twice the maximum hypocentral depth. Placing the stations at greater distance would not improve the network performance, as will be shown in section 5. The station perimeter was then filled by a grid of possible station locations with a spacing of 100 m, which is enough to cover the low-noise areas within the city. With decreasing station spacing the computational costs increase since a larger number of network configurations has to be tested. Locations where it would be impossible to install a station, e.g. in water bodies, were already excluded from this grid.

The final set-up of the input data, generated by pyNetOpt3D and used by the binaries of Antuens et al. (2023) for the optimization, is shown in Fig. 6.

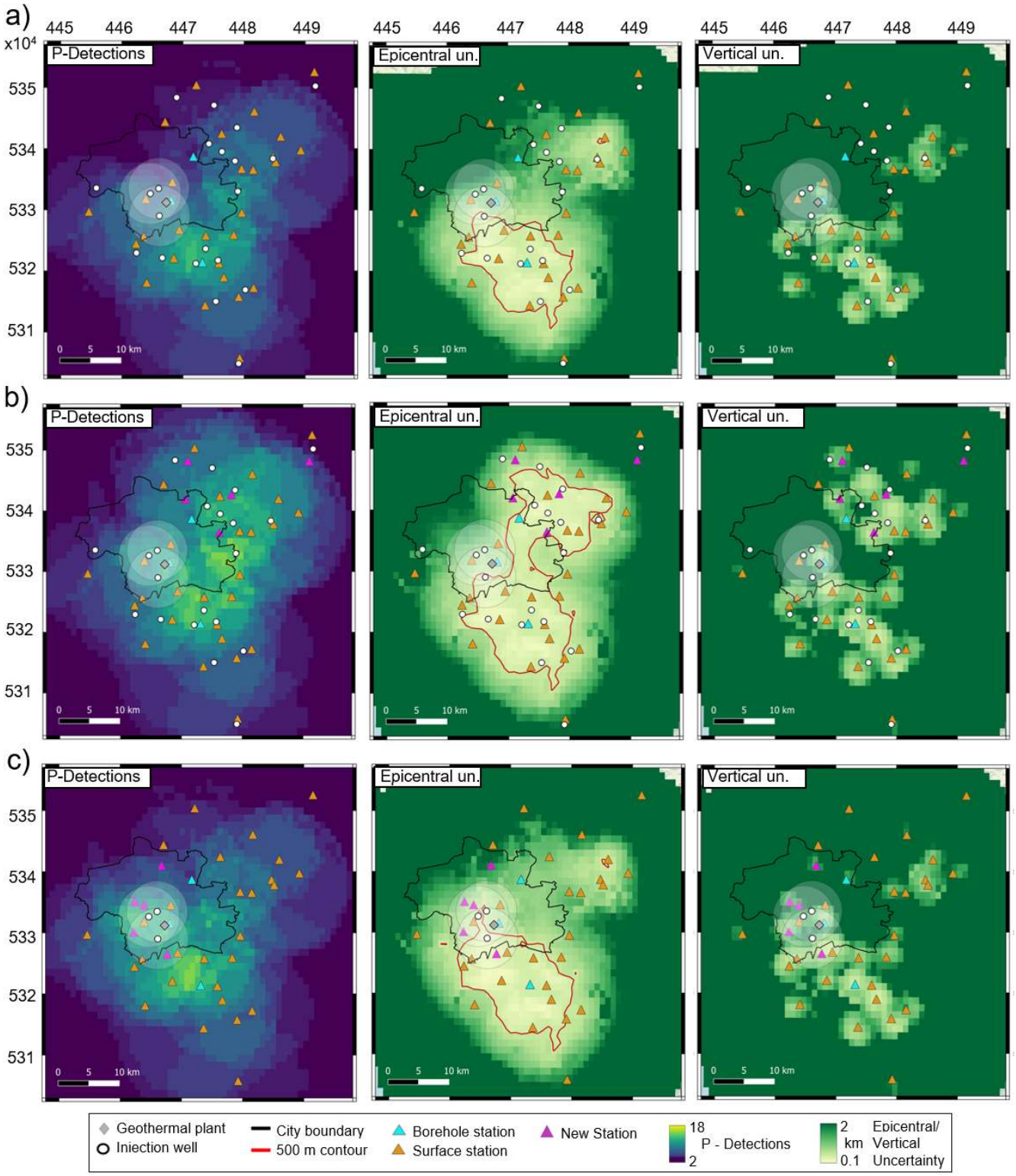

Figure 7 Evaluation of monitoring performance for a M_W 1.3 event at 3 km depth. The performance of the a) existing network, b) optimized network with 5 new stations under consideration of all re-injection wells in the region, c) optimized network with 5 new stations and focus on the three inner-city re-injection wells, is shown. The panels from left to right show the number of P-arrival detections (i.e., recordings with SNR ≥ 5), the epicentral uncertainty and the vertical uncertainty. The location of the inner-city geothermal power plant SLS is plotted. The shaded circles around the three SLS re-injection wells mark a radius of 5 km. The red outline in the epicentral uncertainty plots mark the 500 m contour line. The coordinate system is Gauss-Krüger (GK4).

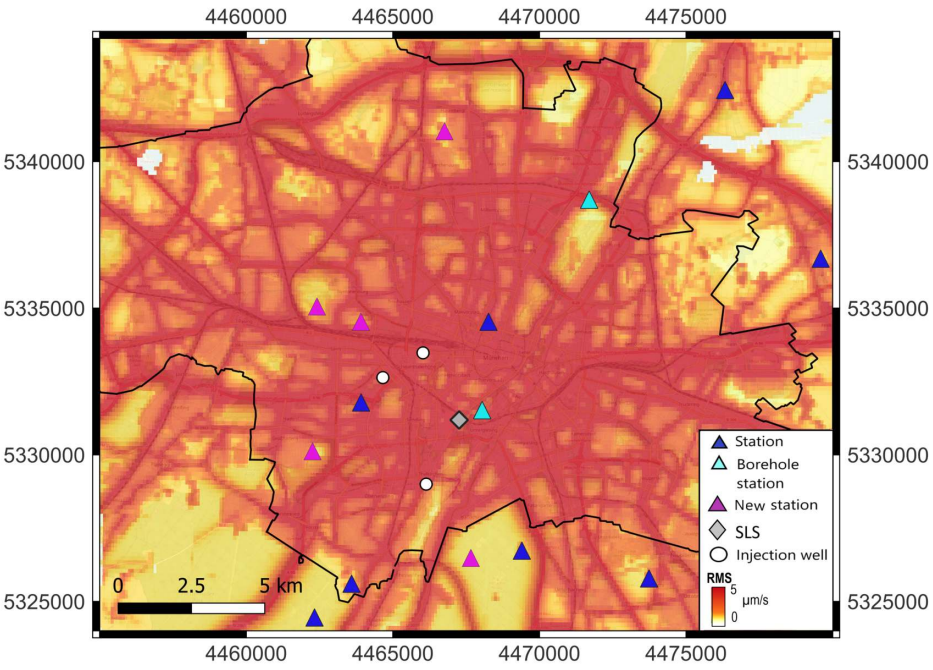

Figure 8 Zoom into the network optimization result for the scenario shown in Fig. 7(c). The pink triangles mark the 5 new surface stations placed by the algorithm. The colors show the computed background noise level as RMS ground velocity. The coordinate system is Gauss-Krüger (GK4).

5 Optimization results and discussion

First of all, the performance of the existing network with a focus on the area surrounding the recently installed SLS power plant is tested using the NetOpt3D program without optimization. The performance in case of a M_W 1.3 event at 3 km depth is tested, which corresponds to the minimum detectable M_W-converted magnitude recommended by the FKPE (Baisch et al., 2012), and is hereafter referred to as target event. The program returns expected location uncertainties and number of detections (i.e., recordings with SNR $\geq$ 5). The largest number of P-wave detections per event is reached for events occurring south of the city-center, while this number decreases significantly in the northeast and in the surrounding of SLS (Fig. 7 a). In the northernmost part of the 5 km radius surrounding SLS, the target events would be detected by even less than 3 stations. Since the source model is implemented based on scaling relations found for Switzerland, the location uncertainties have to be calibrated using recorded events at the geothermal plants in the southern part of the study area (Megies and Wassermann, 2014). To obtain comparable epicentral and vertical uncertainties, the computed values are divided by a factor of three. In this case, the threshold for the FKPE-recommended epicentral uncertainty of < 500 m is only reached south of the city-center, while in the vicinity of SLS epicentral uncertainties of more than 2 km are computed. The 2 km threshold for the vertical uncertainty is once more mostly reached south of the city-center. In general, the poor performance of the existing network in the SLS area can be explained by 1) a lack of monitoring stations in the northwest and a consequent azimuthal gap in this region and 2) the high noise levels in the inner-city, which cause low-SNR recordings resulting in poor onset-time precision and consequently higher location uncertainties.

Considering these observations, we next evaluate how to improve the seismic network by adding new stations. We perform an optimization run for the randomly chosen number of 5 new surface stations, implementing the input data as shown in Fig. 6. The NetOpt3D program performs the simulated annealing and returns the optimal locations for these 5 new stations (Fig. 7 b). All the new stations are placed in the north-northeast, which increases the number of P-wave detections and decreases the epicentral and vertical uncertainties in this area significantly. Nevertheless, in the vicinity of SLS the performance only slightly improved, since none of the stations was placed in the city center. The algorithm placed most of the stations in the north-northeast as the noise levels are lower compared to the city-center and the code tends to locate stations in the quietest sites only (Kraft et al., 2013). Furthermore, it resulted in the largest improvement of the network performance since the improved SNR at a quiet site overrules the lower SNR at a geometrically more optimal site (Kraft et al., 2013). In order to improve the network specifically in the city center, we perform a new optimization run with 5 new surface stations, but only considering the three SLS reinjection wells as event locations. Therefore, the grid of possible station locations only samples the city center. This time the algorithm places the 5 stations closer to SLS (Fig. 7 c). Accordingly, the number of P-wave detections increases in this region. In addition, the epicentral and vertical uncertainties decrease, however, it is not enough to reach the FKPE-recommended location accuracy. The reason are the relatively low SNR values, which results in a poor onset-time precision. Again,

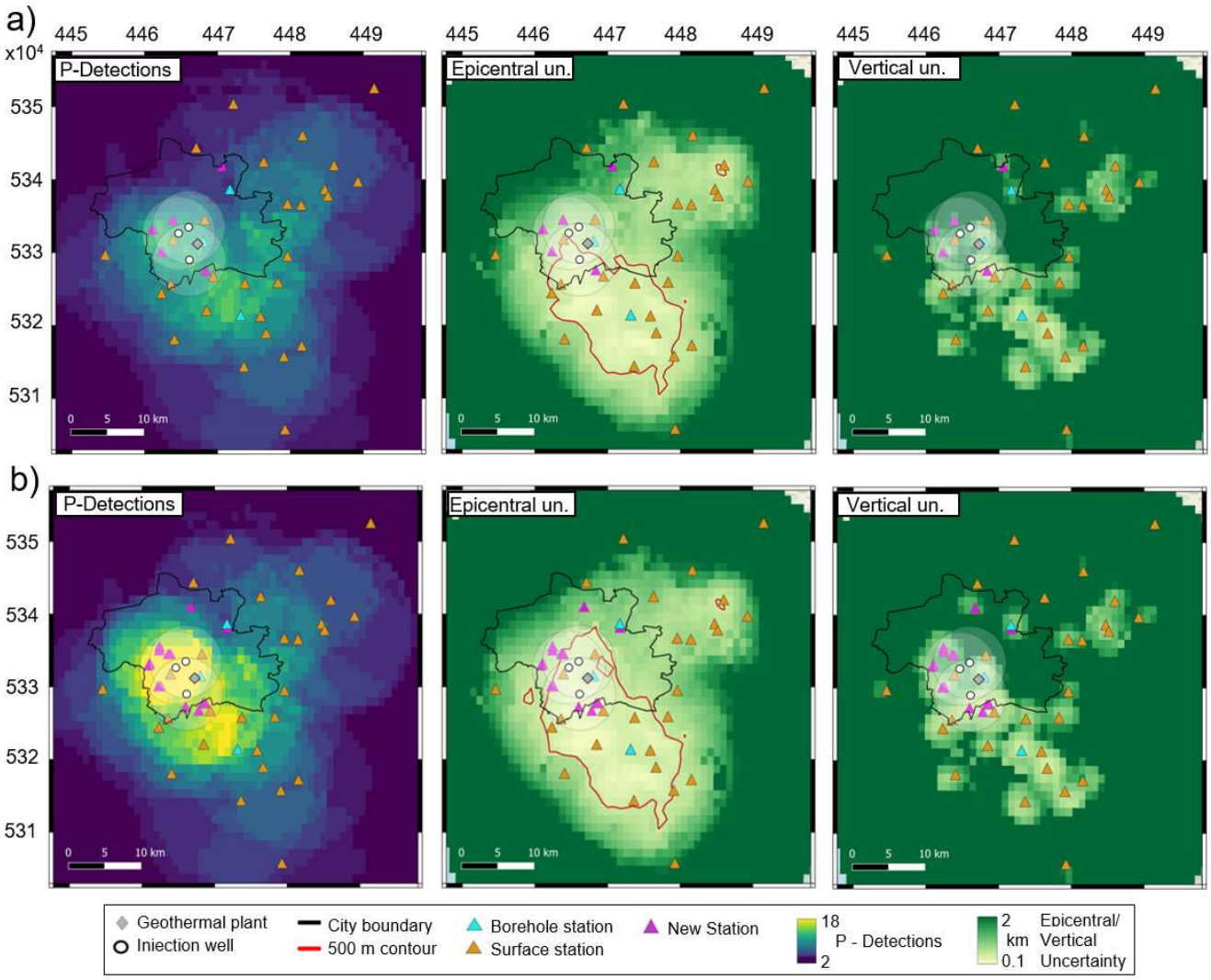

Figure 9 Evaluation of monitoring performance for a M_W 1.3 event at 3 km depth. The performance of the a) optimized network with 5 new stations considering a station perimeter of 12 km and focus on the three inner-city re-injection wells, b) optimized network with 15 new stations and focus on the three inner-city re-injection wells, is shown. The panels from left to right show the number of P-arrival detections (i.e., recordings with SNR $\geq$ 5), the epicentral uncertainty and the vertical uncertainty. The location of the inner-city geothermal power plant SLS is plotted. The shaded circles around the three SLS re-injection wells mark a radius of 5 km. The red outline in the epicentral uncertainty plots mark the 500 m contour line. The coordinate system is Gauss-Krüger (GK4).

the algorithm places the new stations in low noise areas (Fig. 8), which mainly correspond to park areas within the city. This highlights the importance of a high-resolution noise map.

To allow the algorithm to choose low-noise areas outside of the city, we increase the station perimeter from 8 km to 12 km. Nevertheless, the algorithm still places four of the new surface stations close to the SLS power plant and only one station closer to the edge of the city (Fig. 9 a). The resulting epicentral and vertical uncertainties are similar to the values in Fig. 7 c). Therefore, we have shown that considering a station perimeter of 8 km is enough, as placing stations at larger distance does not improve the monitoring performance significantly. This is most likely related to the decreasing amplitude of the ground motion away from the epicenter.

To see if a larger number of surface stations could reach the recommended location precision, the same optimization run is performed using 15 new stations (Fig. 9 b). The number of P-wave detections significantly increases. Nevertheless, even though the epicentral and vertical uncertainties improve it is not sufficient to reach the FKPE-recommended location precision in the vicinity of SLS. In fact, adding even more stations does not significantly improve the location precision any further.

In order to increase the SNR and allow a more accurate determination of the event location, borehole stations are considered in the next step of the optimization. In section 3 the 180m-deep borehole station SYBAD was compared to the overlying surface station SYBOB. We observed that for the vertical component the noise level in the borehole is a factor of 10 lower than at the surface. Therefore, to simulate the noise level for borehole stations in Munich we divide the noise model by a factor of 10 and input it into the NetOpt3D program. Then a net-

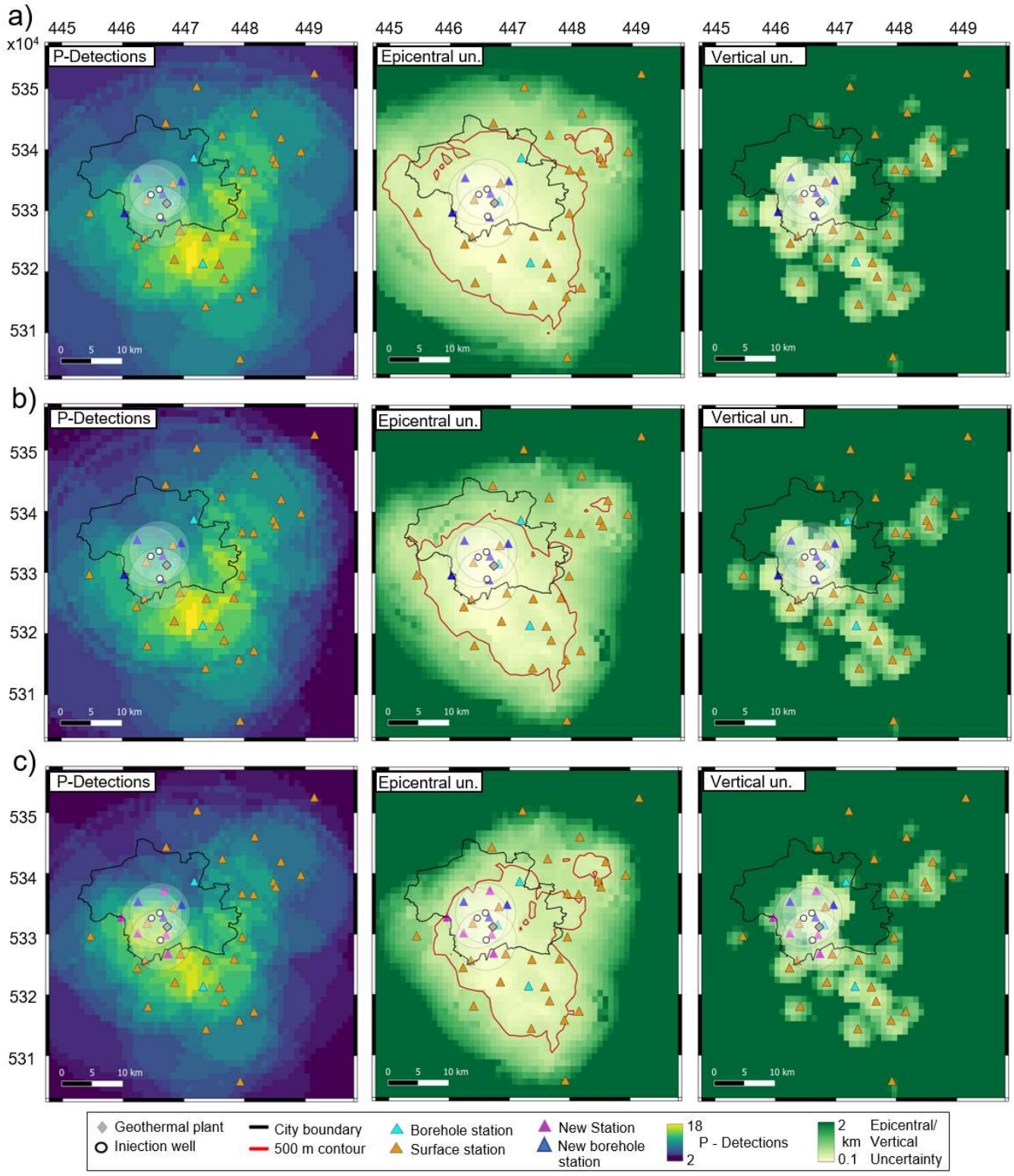

Figure 10 Evaluation of monitoring performance for a M_W 1.3 event at 3 km depth. The performance of the a) optimized network with 5 new 180m-deep borehole stations and focus on the three inner-city re-injection wells, b) optimized network with 5 new 36m-deep borehole stations and focus on the three inner-city re-injection wells, c) optimized network with 3 new 180m-deep borehole stations and 5 new surface stations and focus on the three inner-city re-injection wells. The panels from left to right show the number of P-arrival detections, the epicentral uncertainty and the vertical uncertainty. The location of the inner-city geothermal power plant SLS is plotted. The shaded circles around the three SLS re-injection wells mark a radius of 5 km. The red outline in the epicentral uncertainty plots mark the 500 m contour line. The coordinate system is Gauss-Krüger (GK4).

work optimization for borehole stations is performed. We find that at least 5 new borehole stations are sufficient to reach the recommended epicentral uncertainty of less than 500 m in the surroundings of the SLS reinjection wells (Fig. 10 a). Additionally, the vertical uncertainty threshold of < 2 km is reached almost within the entire 5 km radius, except for some outermost parts.

To estimate the minimum required borehole depth we stepwise decrease the borehole noise level factor for the background noise map. We find that a factor of 6 is sufficient to reach the recommended location accuracy (Fig. 10 b). Assuming the simple relation of noise decreasing with depth by a factor of $\sqrt{depth[m]}$ this would correspond to a borehole depth of 36 m.

Even though borehole stations significantly improve the quality of the monitoring network, their installation is not always feasible due to high costs and infrastructural limitations. Therefore, we test if less borehole stations in combination with additional surface stations could also reach the FKPE-recommended location precision. At first, the optimization is performed for 3 new borehole stations by scaling the noise map with a factor 10. This is followed by an optimization run with 5 new surface stations, while fixing the previously determined borehole stations. The recommended epicentral and vertical uncertainty thresholds are reached in this case (Fig. 10 c).

6 Conclusion

We performed a network optimization using the python wrapper pyNetOpt3D around the NetOpt3D program in order to improve the microseismic monitoring for a safe operation of deep geothermal plants in Munich's innercity. In the first step we constructed a noise model for the Munich area in order to capture the heterogeneous noise conditions. This high resolution noise model enabled the algorithm to find suitable station locations even within the city center. The results suggest that the current monitoring network is not suitable to locate M_L 1 earthquakes with a FKPE-recommended epicentral uncertainty of < 500 m and vertical uncertainty of < 2 km. We showed that adding solely surface stations to the inner-city network is not sufficient to reach the recommended thresholds. The addition of borehole stations significantly improved the quality of the monitoring network, which indicates that borehole installations may be indispensable in urban environments. However borehole installations are not always feasible and come with high costs. We were able to show that a combination of new borehole and new surface stations can be used to record and locate M_L 1 events in Munich with the recommended location precision. This study presents procedures and shows solutions for improving the microseismic monitoring within urban areas both for induced and natural seismicity. Nevertheless, we emphasise that proper seismic monitoring is only one component of a comprehensive risk governance strategy for induced seismicity.

Acknowledgements

This work was supported by the research project SEIGER (Project no. 03EE44003G), funded by the German Federal Ministry of Economic Affairs and Climate Action and managed by the research institute Jülich (PTJ). T. Megies was supported by the GEOBEST-CH project of the Swiss Seismological Service funded by the Swiss Energy Program of the Swiss Federal Office of Energy for the development of pyNetOpt3D. The authors thank the reviewer Anthony Lomax for the helpful comments, which improved the manuscript.

Data and code availability

The Geographical base data from the Bavarian administration for geographical surveying (Geobasisdaten Bayerische Vermessungsverwaltung 2017) was requested at https://www.ldbv.bayern.de/ (last request July 30, 2017). The OpenStreetMap data were downloaded from https://www.openstreetmap.org/export#map=11/48.0290/11.6331 (last request July 29, 2017). The traffic volume data from the city of Munich for 2019 were searched at https://stadt.muenchen.de/infos/verkehrsdaten.html (last accessed July 10, 2020). The pyNetOpt3D code and the binaries of NetOpt3D from Antuens et al. (2023) are available at Zenodo (https://doi.org/10.5281/zenodo.7638856).

Competing interests

The authors have no competing interests.

References

Agemar, T., Weber, J., and Schulz, R. Deep geothermal energy production in Germany. *Energies*, 7(7):4397–4416, 2014. doi: 10.3390/en7074397.

Aki, K. Signal to noise ratio in seismic measurements. *Volcanoes and Tectonos· phere, Tokai Univ. Press, Tokyo*, pages 187–192, 1976.

Antuens, V., Toledo, T., Kraft, T., Reyes, C., and Megies, T. Optimal Design and Ground Truth Performance Test for Deep Geothermal Seismic Monitoring Networks. (in preparation). 2023.

Asten, M. W. and Henstridge, J. Array estimators and the use of microseisms for reconnaissance of sedimentary basins. *Geophysics*, 49(11):1828–1837, 1984. doi: 10.1190/1.1441596.

Baisch, S., Fritschen, R., Groos, J., Kraft, T., Plenefisch, T., Plenkers, K., Ritter, J. R., and Wassermann, J. Empfehlungen zur Überwachung induzierter Seismizität-Positionspapier des FKPE. *DGG Mitteilungen*, (3):17–31, 2012.

Bartal, Y., Somer, Z., Leonard, G., Steinberg, D. M., and Horin, Y. B. Optimal seismic networks in Israel in the context of the Comprehensive Test Ban Treaty. *Bulletin of the seismological society of America*, 90(1):151–165, 2000. doi: 10.1785/0119980164.

Bayerisches Landesamt für Umwelt. Geothermische Charakterisierung von Karst-Kluft-Aquiferen im Großraum München. *Endbericht*, 2012.

Bondár, I., Myers, S. C., Engdahl, E. R., and Bergman, E. A. Epicentre accuracy based on seismic network criteria. *Geophysical Journal International*, 156(3):483–496, 2004. doi: 10.1111/j.1365-246X.2004.02070.x.

Bormann, P. and Wielandt, E. Seismic signals and noise. In *New manual of seismological observatory practice 2 (NMSOP2)*, pages 1–62. Deutsches GeoForschungsZentrum GFZ, 2013. doi: 10.2312/GFZ.NMSOP-2_ch4.

Brune, J. N. Tectonic stress and the spectra of seismic shear waves from earthquakes. *Journal of geophysical research*, 75 (26):4997–5009, 1970. doi: 10.1029/JB075i026p04997.

Büttner, G., Feranec, J., Jaffrain, G., Mari, L., Maucha, G., and Soukup, T. The CORINE land cover 2000 project. *EARSeL eProceedings*, 3(3):331–346, 2004.

Coles, D. and Curtis, A. Efficient nonlinear Bayesian survey design using DN optimization. *Geophysics*, 76(2):Q1–Q8, 2011. doi: 10.1190/1.3552645.

De Landro, G., Picozzi, M., Russo, G., Adinolfi, G. M., and Zollo, A. Seismic networks layout optimization for a high-resolution monitoring of induced micro-seismicity. *Journal of Seismology*, 24:953–966, 2020. doi: 10.1007/s10950-019-09880-9.

D'Alessandro, A., Luzio, D., D'Anna, G., and Mangano, G. Seismic network evaluation through simulation: An application to the Italian National Seismic Network. *Bulletin of the Seismological Society of America*, 101(3):1213–1232, 2011. doi: 10.1785/0120100066.

Edwards, B., Fäh, D., and Giardini, D. Attenuation of seismic shear wave energy in Switzerland. *Geophysical Journal International*, 185(2):967–984, 2011. doi: 10.1111/j.1365-246X.2011.04987.x.

Eulenfeld, T. and Wegler, U. Measurement of intrinsic and scattering attenuation of shear waves in two sedimentary basins and comparison to crystalline sites in Germany. *Geophysical Journal International*, 205(2):744–757, 2016. doi: 10.1093/gji/ggw035.

Evans, K. F., Zappone, A., Kraft, T., Deichmann, N., and Moia, F. A survey of the induced seismic responses to fluid injection in geothermal and CO2 reservoirs in Europe. *Geothermics*, 41: 30–54, 2012. doi: 10.1016/j.geothermics.2011.08.002.

Fowler, C. M. R. *The solid earth: an introduction to global geophysics*. Cambridge University Press, 1990.

Groos, J. and Ritter, J. Time Domain Classification and Quantification of Seismic Noise. In *Noise and diffuse wavefields: extended abstracts of the Neustadt workshop; Neustadt an der Weinstraße, Germany, 5-8 July 2009. Ed.: Ch. Sens-Schönfelder*, page 25, 2009. doi: 10.1111/j.1365-246X.2009.04343.x.

Grünthal, G. and Wahlström, R. An M w based earthquake catalogue for central, northern and northwestern Europe using a hierarchy of magnitude conversions. *Journal of seismology*, 7: 507–531, 2003. doi: 10.1023/B:JOSE.0000005715.87363.13.

Hardt, M. and Scherbaum, F. The design of optimum networks for aftershock recordings. *Geophysical Journal International*, 117 (3):716–726, 1994. doi: 10.1111/j.1365-246X.1994.tb02464.x.

Häring, M. O., Schanz, U., Ladner, F., and Dyer, B. C. Characterisation of the Basel 1 enhanced geothermal system. *Geothermics*, 37(5):469–495, 2008. doi: 10.1016/j.geothermics.2008.06.002.

Havskov, J., Ottemöller, L., Trnkoczy, A., and Bormann, P. Seismic networks. In *New Manual of Seismological Observatory Practice 2 (NMSOP-2)*, pages 1–65. Deutsches GeoForschungsZentrum GFZ, 2012. doi: 10.2312/GFZ.NMSOP-2_ch8.

Hecht, C. and Pletl, C. Das Verbundprojekt GRAME–Wegweiser für eine geothermische Wärmeversorgung urbaner Ballungsräume. *Geothermische Energie*, 82(2):02, 2015.

Hirschberg, S., Wiemer, S., and Burgherr, P. *Energy from the Earth: Deep Geothermal as a Resource for the Future?*, volume 62. vdf Hochschulverlag AG, 2014.

Kijko, A. An algorithm for the optimum distribution of a regional seismic network—I. *pure and applied geophysics*, 115(4): 999–1009, 1977. doi: 10.1007/BF00881222.

Kirkpatrick, S., Gelatt Jr, C. D., and Vecchi, M. P. Optimization by simulated annealing. *science*, 220(4598):671–680, 1983. doi: 10.1126/science.220.4598.671.

Kraft, T. A high-resolution ambient seismic noise model for Europe. *EGU General Assembly, EGU2014-2282*, 27, 2014.

Kraft, T. A high-resolution and calibrated model of man-made seismic noise for Europe. *Jahrestagung der Deutschen Geophysikalischen Gesellschaft*, pages S2–A, 2016.

Kraft, T., Mignan, A., and Giardini, D. Optimization of a large-scale microseismic monitoring network in northern Switzerland. *Geophysical Journal International*, 195(1):474–490, 2013. doi: 10.1093/gji/ggt225.

Kraft, T., Roth, P., and Wiemer, S. Good Practice Guide for Managing Induced Seismicity in Deep Geothermal Energy Projects in Switzerland: Version 2. 2020. doi: 10.3929/ethz-b-000453228.

Lentsch, D. and Schweingruber, M. First Multilateral Deep Geothermal Well in the South German Molasse Basin. *Eropean Geothermal Congress*, 2022.

Lomax, A., Michelini, A., Curtis, A., and Meyers, R. Earthquake location, direct, global-search methods. *Encyclopedia of complexity and systems science*, 5:2449–2473, 2009.

Lund, J. W. and Toth, A. N. Direct utilization of geothermal energy 2020 worldwide review. *Geothermics*, 90:101915, 2021. doi: 10.1016/j.geothermics.2020.101915.

Mahani, A. B., Kao, H., Walker, D., Johnson, J., and Salas, C. Performance evaluation of the regional seismograph network in northeast British Columbia, Canada, for monitoring of induced seismicity. *Seismological Research Letters*, 87(3):648–660, 2016. doi: 10.1785/0220150241.

Megies, T. and Wassermann, J. Microseismicity observed at a non-pressure-stimulated geothermal power plant. *Geothermics*, 52: 36–49, 2014. doi: 10.1016/j.geothermics.2014.01.002.

Megies, T. and Wassermann, J. Verbundprojekt MAGS2 - Vom Einzelsystem zur großräumigen Nutzung- EP2: Untersuchungen zur optimierten seismischen Überwachung hydrogeothermaler Systeme bei dichter räumlicher Lage der Bohrerlaubnisfelder am Beispiel der Situation im Süden Münchens. *Abschlussbericht*, 2017.

Megies, T., Kraft, T., and Reyes, C. pyNetOpt3D. *Zenodo*, https://doi.org/10.5281/zenodo.7638856, 2023.

Myers, S. C. and Schultz, C. A. Improving sparse network seismic location with Bayesian kriging and teleseismically constrained calibration events. *Bulletin of the Seismological Society of America*, 90(1):199–211, 2000. doi: 10.1785/0119980171.

Neuffer, T. and Kremers, S. How wind turbines affect the performance of seismic monitoring stations and networks. *Geophysical Journal International*, 211(3):1319–1327, 2017. doi: 10.1093/gji/ggx370.

Podvin, P. and Lecomte, I. Finite difference computation of traveltimes in very contrasted velocity models: a massively parallel approach and its associated tools. *Geophysical Journal International*, 105(1):271–284, 1991. doi: 10.1111/j.1365-246X.1991.tb03461.x.

Riedl, C. A Seismic Noise Map for the Greater Munich Area. Master's thesis, LMU Munich, 2017.

Schmittbuhl, J., Lambotte, S., Lengliné, O., Grunberg, M., Jund, H., Vergne, J., Cornet, F., Doubre, C., and Masson, F. Induced and triggered seismicity below the city of Strasbourg, France from November 2019 to January 2021. *Comptes Rendus. Géoscience*, 353(S1):561–584, 2021. doi: 10.5802/crgeos.71.

Seithel, R., Gaucher, E., Mueller, B., Steiner, U., and Kohl, T. Probability of fault reactivation in the Bavarian Molasse Basin. *Geothermics*, 82:81–90, 2019. doi: 10.1016/j.geother-

mics.2019.06.004.

Shannon, C. E. A mathematical theory of communication. *The Bell system technical journal*, 27(3):379–423, 1948. doi: 10.1002/j.1538-7305.1948.tb01338.x.

Stabile, T., Iannaccone, G., Zollo, A., Lomax, A., Ferulano, M., Vetri, M., and Barzaghi, L. A comprehensive approach for evaluating network performance in surface and borehole seismic monitoring. *Geophysical Journal International*, 192(2):793–806, 2013. doi: 10.1093/gji/ggs049.

Steinberg, D. M. and Rabinowitz, N. Optimal seismic monitoring for event location with application to on site inspection of the comprehensive nuclear test ban treaty. *Metrika*, 58(1):31–57, 2003. doi: 10.1007/s001840200222.

Wawerzinek, B., Buness, H., von Hartmann, H., and Tanner, D. C. S-wave experiments for the exploration of a deep geothermal carbonate reservoir in the German Molasse Basin. *Geothermal Energy*, 9(1):1–21, 2021. doi: 10.1186/s40517-021-00189-w.